Adaptive Voltage and Frequency Control of Islanded Multi-Microgrids

David Ofosu Amoateng, *Student Member, IEEE*, Mohamed Al Hosani, *Member, IEEE*, Mohamed Shawky Elmoursi, *Senior Member, IEEE*, Konstantin Turitsyn, *Member, IEEE*, and James L. Kirtley, Jr., *Life Fellow, IEEE*

***Abstract*—This paper introduces an adaptive voltage and frequency control method for inverter-based distributed generations (DGs) in a multi-microgrid (MMG) structure using distributed cooperative control and adaptive neural networks (ANN). First, model-based controllers are designed using the Lyapunov theory and dynamics of the inverter-based DGs. ANNs are then utilized to approximate these dynamics, resulting in an intelligent controller, which does not require *a priori* information about DG parameters. Also, the proposed controllers do not require the use of voltage and current proportional-integral controllers normally found in the literature. The effectiveness of the proposed controllers are verified through simulations under different scenarios on an MMG test system. Using Lyapunov analysis, it is proved that the tracking error and the neural network weights are uniformly ultimately bounded, which results in achieving superior dynamic voltage and frequency regulation.**

***Index Terms*—Adaptive neural networks (ANNs), cooperative control, distributed generation (DG), Lyapunov theory, multi-microgrid (MMG).**

Nomenclature

DG	Distributed generation.
MMG	Multi-microgrid.
ANN	Adaptive neural networks.
PI	Proportional Integral.
VCVSI	Voltage-controlled voltage source inverter.
${v_{odi}}^*$	Voltage generated by droop control.
ω_i	Angular frequency generated by droop control.
n_{Qi}	$Q-V$ droop coefficient.
m_{Pi}	$P-F$ droop coefficient.
v_{ni}	Nominal value of DG output voltage.
ω_{ni}	Nominal value of DG angular frequency.
Q_i	Filtered output reactive power.
P_i	Filtered output active power.
v_{odi}, v_{oqi}	Direct and quadrature component of DG output voltage.
i_{ldi}, i_{lqi}	Direct and quadrature component of DG inductor current.
v_{idi}, v_{iqi}	Direct and quadrature component of inverter output voltage.
i_{odi}, i_{oqi}	Direct and quadrature component of DG output current.
v_{bdi}, v_{bqi}	Direct and quadrature component of DG bus voltage.
r_{fi}, L_{fi}, C_{fi}	Resistance, inductance and capacitance of LC filter.
r_c, L_c	Resistance and inductance of the coupling line.

Manuscript received June 18, 2017; revised October 15, 2017; accepted November 26, 2017. Date of publication December 7, 2017; date of current version June 18, 2018. Paper no. TPWRS-00915-2017. *(Corresponding author: David Ofosu Amoateng.)*

D. O. Amoateng, M. Al Hosani, and M. S. Elmoursi are with the Department of Electrical and Computer Engineering, Masdar Institute, Khalifa University of Science and Technology, Abu Dhabi 54224, United Arab Emirates (e-mail: amoat7@gmail.com; mohalhosani@masdar.ac.ae; melmoursi@masdar.ac.ae).

K. Turitsyn is with the Department of Mechanical Engineering, Massachusetts Institute of Technology, Cambridge, MA 02139 USA (e-mail: turitsyn@mit.edu).

J. L. Kirtley, Jr. is with the Department of Electrical Engineering and Computer Science, Massachusetts Institute of Technology, Cambridge, MA 02139 USA (e-mail: kirtley@mit.edu).

Color versions of one or more of the figures in this paper are available online at http://ieeexplore.ieee.org.

Digital Object Identifier 10.1109/TPWRS.2017.2780986

I. Introduction

To ENSURE effective and stable operation of microgrids, they should be equipped with suitable control algorithms, which satisfy operational constraints and maximize performance. There are basically three levels of hierarchical control in a microgrid that ensure reliable operation: primary, secondary and tertiary control. The conventional primary droop control maintains the microgrid's voltage and frequency in islanded mode, offers plug and play capability for the DGs and shares the active and reactive power among the DGs without using communication links. However, it can cause frequency and voltage deviations [1]–[3]. A secondary control action is therefore used to restore the microgrid's voltage and frequency to nominal values. The third level of control, tertiary control, deals with economic dispatch and power flows between the microgrid and the main grid [4], [5].

Two main control architectures exist for secondary control: centralized and distributed. The former requires a central controller which communicates with all the DGs and is responsible for control and coordination. The centralized control structure however creates reliability concerns, as the whole system can collapse following the failure of the central controller. This single point of failure can be mitigated by duplicating the controller [6]. A secondary voltage and frequency controller for a microgrid using distributed control is proposed in [7]. The DGs communicate with each other based on a directed graph (digraph) and their controllers only require local information from neighbouring DG units for the control action, with the cooperative team objective defined in terms of an error function. The authors in [7] also show that by changing the synchronizing gain, the response speed of the secondary controller action is affected. A distributed averaging method is proposed in [8], to regulate the voltage and frequency of a microgrid to nominal values, while maintaining good reactive power sharing among the DGs. The averaging method tunes the voltage controller and provides a simple trade-off between conflicting goals of sharing reactive power and regulating bus voltages. Though the distributed averaging method depends on extensive communication links, the authors did not consider the effects of latency on the performance of the controller.

One major limitation of the conventional secondary voltage control method is that it yields poor reactive power sharing among the DGs in a microgrid. When secondary voltage control is applied, the DGs voltage magnitudes are restored to a reference value. This however changes the inverter reactive power injections and, therefore, worsens the reactive power sharing of the DGs [8], [9]. Sharing the reactive power proportionally also changes the output voltages of the DGs. Therefore, conventional secondary control cannot restore voltages to rated values while sharing reactive power proportionally.

A secondary voltage control method using feedback linearization and distributed control is proposed in [10]. Using input-output feedback linearization, the secondary voltage control is converted to a second-order tracking synchronization problem. The authors in [10] however, did not consider secondary frequency control and the effects of their proposed secondary voltage control on reactive power sharing among the DGs. In [11], a centralized secondary control method to achieve equal reactive power sharing among the DGs in a microgrid is proposed. The controller consists of an external loop using a low bandwidth communication network. Equal reactive power sharing will however result in poor voltage regulation due to mismatched feeder impedances between the DGs and the loads. The use of the central controller also results in a single point of failure of the system. An accurate reactive power sharing scheme for an islanded microgrid was developed and tested on a 2kVA test system in [12]. The control strategy tunes adaptive virtual impedances to correct the voltage drop mismatches across the feeders. The control method exhibits good performance for reactive power sharing. However, it is not easy to obtain the adaptive coefficients. Also, this secondary control action exhibits a lower voltage than the conventional droop control method. A two-layer distributed cooperative controller is also proposed in [13]. The first control layer consists of voltage source inverters which are responsible for providing voltage and frequency support to the microgrid. The first layer also contains secondary voltage and frequency controllers which eliminate the voltage and frequency deviations of droop control. The current source inverters in the second layer are responsible for controlling only the active and reactive power flows. However, this control method is very complex and depends heavily on system dynamics and DG parameters.

In this paper, the aim is to approximate these dynamics using artificial neural networks and also to simplify the multiple layers of control usually found in published works. Neural networks are basically mathematical models which are analogous to the observed behaviour of biological brain's neurons. They have been exploited to solve a number of tasks such as approximating dynamics of robotic manipulators [14], [15], recognizing handwritten digits [16] and load forecasting [17], [18]. In [19], neural networks are used to determine the optimal tilt angle of PV panels in order to absorb maximum energy from the sun. The optimal tilt angle is a non-linear function of location, time of year and ground reflectivity. The neural network approximates this function and hence maximizes the amount of power produced by the PVs.

Therefore, the main contributions of this paper are as follows:

i) Adaptive neural networks and cooperative control theory are used to develop primary and secondary voltage and frequency controllers for inverter-based DGs in a multi-microgrid structure. The proposed controllers replace the conventional voltage and current PI controllers with a single level of control, resulting in a simple controller that can be deployed on inverter-based DGs.
ii) The controllers developed are less dependent on system dynamics, maintain the voltage and frequency near nominal values, achieve good active and reactive sharing among the DGs in the multi-microgrid and are more robust with respect to latency and power system disturbances.

II. Preliminaries and Problem Formulation

A. Dynamical Model of an Inverter-Based DG

The controllers are designed using the droop control equations and the differential equations of the LC filter and the coupling inductor. The droop characteristics for the ith DG are given by [20]

$$v^*_{odi} = v_{ni} - n_{Qi}Q_i \tag{1}$$

$$\omega_i = \omega_{ni} - m_{Pi}P_i. \tag{2}$$

For the VCVSI, the differential equations of the LC filter and the coupling inductor are given by [21]

$$\dot{i}_{ldi} = \frac{-r_{fi}}{L_{fi}}i_{ldi} + \omega_i i_{lqi} + \frac{1}{L_{fi}}v_{idi} - \frac{1}{L_{fi}}v_{odi} \tag{3}$$

$$\dot{i}_{lqi} = \frac{-r_{fi}}{L_{fi}}i_{lqi} - \omega_i i_{ldi} + \frac{1}{L_{fi}}v_{iqi} - \frac{1}{L_{fi}}v_{oqi} \tag{4}$$

$$\dot{v}_{odi} = \omega_i v_{oqi} + \frac{1}{C_{fi}}i_{ldi} - \frac{1}{C_{fi}}i_{odi} \tag{5}$$

$$\dot{v}_{oqi} = -\omega_i v_{odi} + \frac{1}{C_{fi}}i_{lqi} - \frac{1}{C_{fi}}i_{oqi} \tag{6}$$

$$\dot{i}_{odi} = \frac{-r_{ci}}{L_{ci}}i_{odi} + \omega_i i_{oqi} + \frac{1}{L_{ci}}v_{odi} - \frac{1}{L_{ci}}v_{bdi} \tag{7}$$

$$\dot{i}_{oqi} = \frac{-r_{ci}}{L_{ci}}i_{oqi} - \omega_i i_{odi} + \frac{1}{L_{ci}}v_{oqi} - \frac{1}{L_{ci}}v_{bqi}. \tag{8}$$

B. Network Model

A digraph is used to model the communication network of the multi-microgrid. A digraph can be expressed as $G = (V, E, A)$ with a non-empty finite set of N nodes $V = \{v_1, v_2, \ldots v_N\}$, a set of edges E and the associated adjacency matrix $A = [a_{ij}] \in \mathbb{R}^{N\times N}$. The DGs are considered as nodes of the communication digraph. An edge from node j to node i is denoted by (v_j, v_i), which means that node i receives information from node j. a_{ij} is the weight of edge (v_j, v_i), and $a_{ij} > 0$ if $(v_j, v_i) \in E$, otherwise $a_{ij} = 0$ [22]. In this paper, the communication links are considered to be unidirectional.

The voltage and frequency control objectives are to regulate the voltage amplitude and frequency to some prescribed or reference value, share the active powers proportionally according to the droop coefficients of the DGs and maintain good reactive power sharing among the DGs. The following definitions, theorems and lemmas will help to achieve this goal.

Definition. Function Approximation: A continuous function $f(x) : \mathbb{R}^n \to \mathbb{R}^m$, can be approximated by an activation function neural network. Then, given a compact set $S \in \mathbb{R}^n$ and a positive constant ϵ_n, there exists a single hidden layer neural network such that $f(x) = W^T\sigma(x) + \epsilon(x)$, where $W \in \mathbb{R}^{l\times p}$ is the neural network weight and ϵ is the neural network approximation error, with $\|\epsilon(x)\| < \epsilon_n, \forall x \in S$ where l is the number of neural network nodes and p is the number of output variables. The radial basis activation function $\sigma(x)$ is defined as

$$\sigma_j(x) = \exp\left[\frac{-(x-\mu_j)^T(x-\mu_j)}{v_j^2}\right], j = 1, 2, ..., l \quad (9)$$

where μ_j and v_j^2 is the center and variance of the function, respectively [15], [23]. Fig. 1 shows the structure of a single hidden layer neural network.

Lemma: Uniform Ultimate boundedness by Lyapunov extension: If for a system $\dot{x} = f(x, t)$, $\exists$ a Lyapunov function $V(x, t)$ such that for x in a compact set $S \subset \mathbb{R}^n$, $V(x, t) > 0$ and $\dot{V}(x, t) < 0$ for some $\|x\| > R$ such that the ball of radius R is contained in S, then the system is uniformly ultimately bounded and the norm of the state is bounded within a neighbourhood of R [24].

Assumption 1: Droop control aligns the output voltage of each DG on the d-axis of the corresponding reference frame. v_{oq} can therefore be assumed to be zero [25].

Assumption 2: For any compact set of $\mathbb{R}^n$, the ideal neural network weights are bounded by known positive values i.e., $\|W\|_F \le W_\beta$ where $\|\cdot\|_F$ denotes the Frobenius norm [26].

III. Control Design

In this section, the proposed voltage and frequency controllers for the DGs are developed using Lyapunov theory and neural networks. These controllers maintain the voltage and frequency, share active power proportionally according to the DG ratings and exhibit good reactive power sharing.

A. Adaptive Voltage Control

A relation between the output voltage variable v_{odi} and the input v_{idi} is first established. From the differential equations of the LC filter and the coupling inductor, differentiating (5) and substituting (3) yields

$$\ddot{v}_{odi} = (L_{fi}C_{fi})^{-1}\Big[\omega_i i_{lqi}L_{fi} - r_{fi}i_{ldi} - v_{odi} - \dot{i}_{odi}L_{fi} + v_{idi}\Big] \quad (10)$$

The cooperative tracking error function e_{1i} is defined as

$$e_{1i} = \sum_{j\in N_i} a_{ij}(v_{odi} - v_{odj}) + g_i(v_{odi} - v_{ref}) + \sum_{j\in N_i} a_{ij}(n_{Qi}Q_i - n_{Qj}Q_j) \quad (11)$$

where $g_i \ge 0$ is non-zero for DGs with the reference value. e_{1i} is defined as such because it is difficult to regulate voltage accurately while sharing reactive power among DGs using their droop coefficients. The error function e_{1i} is therefore selected as above to enforce some compromise between voltage regulation and reactive power sharing among the DGs. The cooperative error function defined above is used for secondary voltage control. For primary control, e_{1i} reduces to $v_{odi} - v_{ref}$. The neural network controller therefore tries to make this error as small as possible. Equation (11) can be written alternatively as

$$e_{1i} = (d_i + g_i)v_{odi} - \sum_{j\in N_i} a_{ij}v_{odj} + g_i v_{ref} + \sum_{j\in N_i} a_{ij}(n_{Qi}Q_i - n_{Qj}Q_j) \quad (12)$$

where d_i is defined as $d_i = \sum_{j\in N_i} a_{ij}$. Another error variable e_{2i} is defined as

$$e_{2i} = (d_i + g_i)\dot{v}_{odi} - \alpha_i \quad (13)$$

where α_i is a virtual control and will be defined later. A Lyapunov function V_{1i} is chosen as

$$V_{1i} = \frac{1}{2}e_{1i}^2 \quad (14)$$

Differentiating V_{1i} and substituting (12) yields

$$\dot{V}_{1i} = e_{1i}\Big[(d_i + g_i)\dot{v}_{odi} - \sum_{j\in N_i} a_{ij}\dot{v}_{odj} + \sum_{j\in N_i} a_{ij}(n_{Qi}\dot{Q}_i - n_{Qj}\dot{Q}_j)\Big] \quad (15)$$

Substituting (13) into (15) yields

$$\dot{V}_{1i} = e_{1i}\Big[(e_{2i} + \alpha_i) - \sum_{j\in N_i} a_{ij}\dot{v}_{odj} + \sum_{j\in N_i} a_{ij}(n_{Qi}\dot{Q}_i - n_{Qj}\dot{Q}_j)\Big] \quad (16)$$

α_i is selected as

$$\alpha_i = -k_{1i}e_{1i} + \sum_{j\in N_i} a_{ij}\dot{v}_{odj} - \sum_{j\in N_i} a_{ij}(n_{Qi}\dot{Q}_i - n_{Qj}\dot{Q}_j) \quad (17)$$

where $\dot{Q}_i = -\omega_{icf} Q_i + \omega_{icf}(v_{oqi} i_{odi} - v_{odi} i_{oqi})$ [21] and ω_{icf} is the cut off frequency of the low pass filter. Substituting (17) into (16) yields

$$\dot{V}_{1i} = e_{1i} e_{2i} - k_{1i} e_{1i}^2. \tag{18}$$

Choosing another Lyapunov function

$$V_{2i} = V_{1i} + \frac{1}{2} \frac{L_{fi} C_{fi}}{d_i + g_i} e_{2i}^2. \tag{19}$$

Differentiating yields

$$\dot{V}_{2i} = \dot{V}_{1i} + e_{2i} \frac{L_{fi} C_{fi}}{d_i + g_i} \left[(d_i + g_i) \ddot{v}_{odi} - \dot{\alpha}_i \right]. \tag{20}$$

Substituting (10) and (18) into (20) yields

$$\dot{V}_{2i} = e_{1i} e_{2i} - k_{1i} e_{1i}^2 + e_{2i} \Bigg[\omega_i i_{lqi} L_{fi} - r_{fi} i_{ldi} - v_{odi} - \dot{i}_{odi} L_{fi} + v_{idi} - \frac{L_{fi} C_{fi}}{d_i + g_i} \dot{\alpha}_i \Bigg]. \tag{21}$$

The model-based controller can therefore be selected as

$$v_{idi} = -e_{1i} - k_{2i} e_{2i} + F_i(x_i) \tag{22}$$

where

$$F_i(x_i) = -\omega_i i_{lqi} L_{fi} + r_{fi} i_{ldi} + v_{odi} + \dot{i}_{odi} L_{fi} + \frac{L_{fi} C_{fi}}{d_i + g_i} \dot{\alpha}_i. \tag{23}$$

According to the Definition in Section II, a neural network can be used to approximate $F_i(x_i)$ as

$$F_i(x_i) = W_i^{*T} \sigma_i(x_i) + \epsilon_i(x_i) \tag{24}$$

where $W_i^{*T} \in \mathbb{R}^{1 \times n}$ is the ideal neural network weight vector, n is the number of neural nodes and $\epsilon_i(x_i)$ is the approximation error. W_i^{*T} is unknown and therefore its estimate $\hat{W}_i^T$ is used to design the secondary voltage controller. The NN controller and its update law is proposed as

$$v_{idi} = -e_{1i} - k_{2i} e_{2i} - \hat{W}_i^T \sigma_i(x_i) \tag{25}$$

$$\dot{\hat{W}}_i = G_i(\sigma_i(x_i) e_{2i} - \kappa_i \| e_{2i} \| \hat{W}_i) \tag{26}$$

where k_{2i} and κ_i are positive constants and $G_i \in \mathbb{R}^{n \times n}$ is diagonal and positive. The input to the neural network is selected as $x_i = [v_{odi} \quad e_{1i} \quad e_{2i} \quad \dot{v}_{odi}]$.

Substituting (18), (24) and (25) into (20) yields

$$\dot{V}_{2i} = -k_{1i} e_{1i}^2 - k_{2i} e_{2i}^2 + \tilde{W}_i^T \sigma_i(x_i) e_{2i} + \epsilon_i(x_i) e_{2i} \tag{27}$$

where $\tilde{W}_i = W_i^* - \hat{W}_i$.

Theorem 1: Given the inverter-based DG system with dynamics as shown in (3) - (8) and the adaptive neural network voltage control law in (25) and its update in (26), the error e_{2i} and the weight estimation errors $\tilde{W}_i$ are uniformly ultimately bounded. Furthermore, e_{2i} can be made small by increasing the gain k_{2i}.

The proof of Theorem 1 is shown in Appendix A.

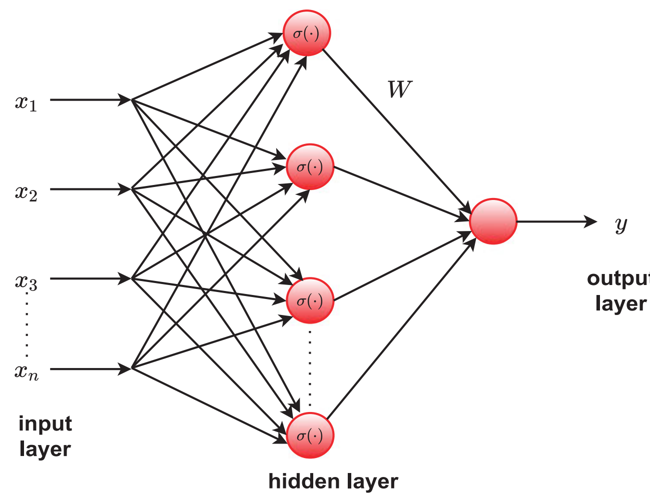

Fig. 1. Single hidden layer neural network structure.

B. Adaptive Frequency Control

In this section, the adaptive frequency controller which synchronizes ω_i to a reference value ω_{ref} while sharing the active powers proportionally among the DGs is developed. Differentiating (2) yields

$$\dot{\omega}_i = \dot{\omega}_{ni} - m_{Pi} \dot{P}_i \tag{28}$$

An error variable $e_{\omega i}$ is defined as

$$e_{\omega i} = (d_i + g_i)\omega_i - \sum_{j \in N_i} a_{ij} \omega_j + g_i \omega_{ref} + \sum_{j \in N_i} a_{ij}(m_{Pi} P_i - m_{Pj} P_j) \tag{29}$$

We select the Lyapunov function V_{fi} as

$$V_{fi} = \frac{1}{2}(d_i + g_i)^{-1} e_{\omega i}^2 \tag{30}$$

Differentiating (30) yields

$$\dot{V}_{fi} = e_{\omega_i}(d_i + g_i)^{-1} \dot{e}_{\omega_i}$$

$$\dot{V}_{fi} = e_{\omega_i} \Bigg[\dot{\omega}_i - (d_i + g_i)^{-1} \sum_{j \in N_i} a_{ij} \dot{\omega}_j + (d_i + g_i)^{-1} \sum_{j \in N_i} a_{ij}(m_{Pi} \dot{P}_i - m_{Pj} \dot{P}_j) \Bigg]. \tag{31}$$

Substituting (28) into (31) yields

$$\dot{V}_{fi} = e_{\omega_i} \Bigg[\dot{\omega}_{ni} - m_{Pi} \dot{P}_i - (d_i + g_i)^{-1} \Bigg\{ \sum_{j \in N_i} a_{ij} \dot{\omega}_j + \sum_{j \in N_i} a_{ij}(m_{Pi} \dot{P}_i - m_{Pj} \dot{P}_j) \Bigg\} \Bigg]. \tag{32}$$

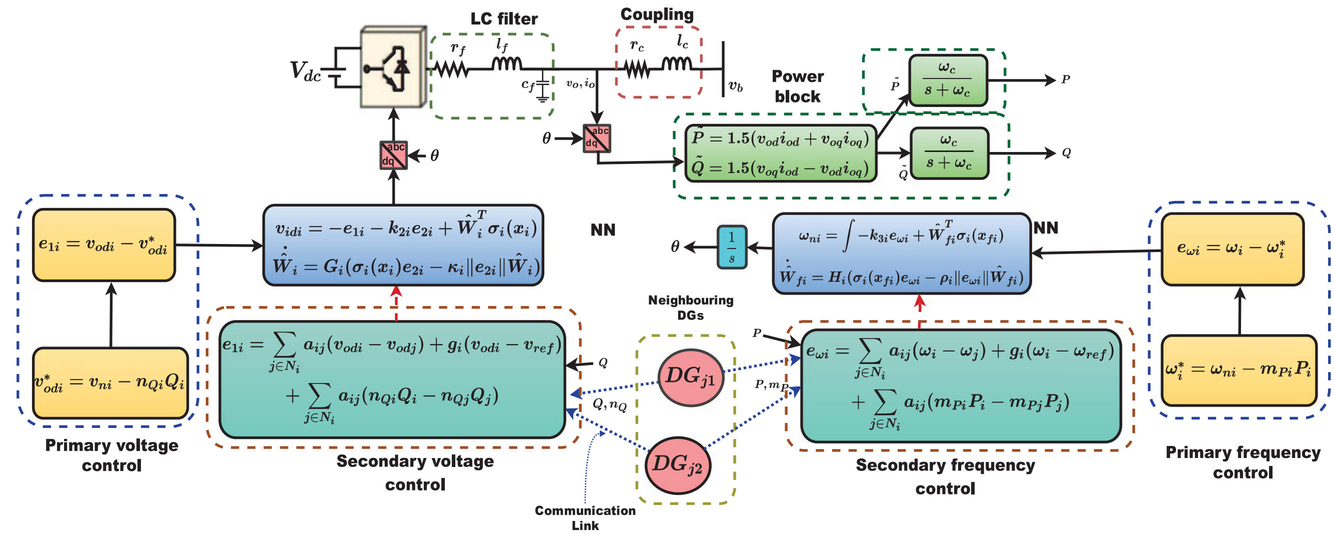

Fig. 2. Block diagram of the proposed adaptive voltage and frequency controller.

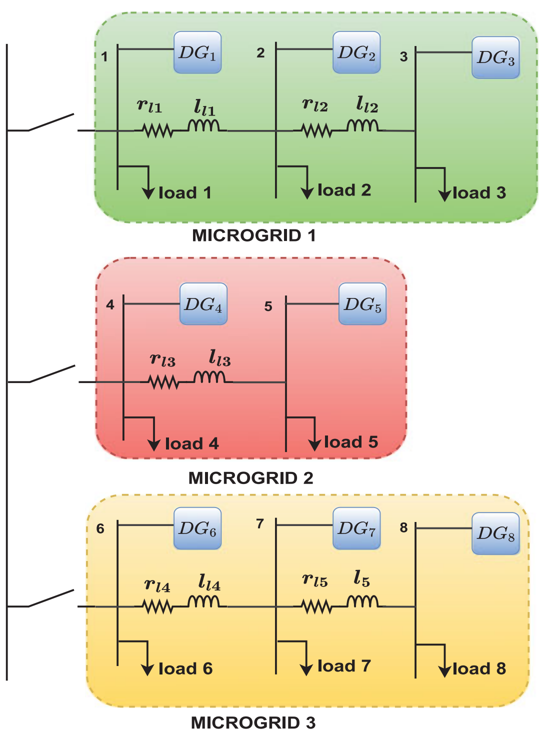

Fig. 3. Multi-microgrid structure.

The input to the model-based frequency controller $\dot{\omega}_{ni}$ is chosen as

$$\dot{\omega}_{ni} = -k_{3i}e_{\omega_i} + m_{Pi}\dot{P}_i + (d_i + g_i)^{-1}\Bigg(\sum_{j\in N_i} a_{ij}\dot{\omega}_j + \sum_{j\in N_i} a_{ij}(m_{Pi}\dot{P}_i - m_{Pj}\dot{P}_j)\Bigg). \tag{33}$$

Then, a neural network is used to approximate the dynamics as

$$W_{fi}^{*}\sigma_i(x_{fi}) = m_{Pi}\dot{P}_i + (d_i + g_i)^{-1}\Bigg[\sum_{j\in N_i} a_{ij}\dot{\omega}_j + \sum_{j\in N_i} a_{ij}(m_{Pi}\dot{P}_i - m_{Pj}\dot{P}_j)\Bigg] - \epsilon_i(x_{fi}). \tag{34}$$

Substituting (33) and (34) into (32) yields

$$\dot{V}_{fi} = -k_{3i}e_{\omega_i} + \tilde{W}_{fi}^{T}\sigma_i(x_{fi})e_{\omega_i} + \epsilon_i(x_{fi})e_{\omega_i}. \tag{35}$$

The adaptive neural network controller for the secondary frequency control and its update laws are written as

$$\dot{\omega}_{ni} = -k_{3i}e_{\omega_i}^{2} - \hat{W}_{fi}^{T}\sigma_i(x_{fi})e_{\omega_i} \tag{36}$$

$$\dot{\hat{W}}_{fi} = R_i(\sigma_i(x_{fi})e_{\omega_i} - \rho_i\|e_{\omega_i}\|\hat{W}_{fi}) \tag{37}$$

where k_{3i}, ρ_i are positive constants and $R_i \in \mathbb{R}^{n\times n}$ is diagonal and positive. The input to the neural network is selected as $x_{fi} = [v_{odi} \quad e_{fi} \quad \omega_i \quad m_{Pi}P_i]$.

Theorem 2: Given the adaptive neural network frequency control law in (36) and its update in (37), the error $e_{\omega i}$ and the weight estimation errors $\tilde{W}_{fi}$ are uniformly ultimately bounded. Furthermore, $e_{\omega i}$ can be made small by increasing the gain k_{3i}.

The proof of Theorem 2 is shown in Appendix B, while Fig. 2 shows the overall block diagram of the proposed adaptive voltage and frequency controller.

IV. Evaluation and Simulation Results

The performance of the proposed adaptive voltage and frequency controllers is verified by simulating an islanded multi-microgrid which consists of eight inverter-based DGs, as depicted in Fig. 3 [27]. MATLAB/Simulink and its SimPower System Library are used to model the MMG structure. The DG, line and load parameters are shown in Tables I and II. The

TABLE I
DG PARAMETERS

	DG 1, 4, 5, 8 (45 KVA)		DG 2, 3, 6, 7 (34 KVA)	
DGs	m_P	0.000094	m_P	0.000125
	n_Q	0.0013	n_Q	0.0015
	R_c	0.03 Ω	R_c	0.03 Ω
	L_c	0.35 mH	L_c	0.35 mH
	R_f	0.1 Ω	R_f	0.1 Ω
	L_f	1.35 mH	L_f	1.35 mH
	C_f	50 μF	C_f	50 μF

TABLE II
LOADS AND LINES PARAMETERS

Loads			Lines		
Bus	P_o(kW)	Q_o(kVAr)		R(Ω)	L(mH)
1	17	15	l_1	0.23	0.35
2	15	12	l_2	0.35	0.68
3	12	8	l_3	0.493	0.494
4	18.5	14	l_4	0.1	0.318
5	16	11	l_5	0.161	0.372
6	20	15			
7	15.3	10			
8	15.6	9.6			

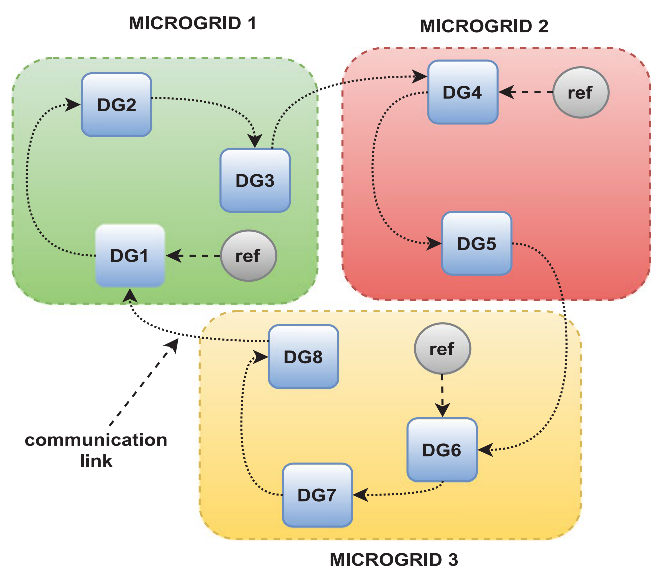

Fig. 4. Communication digraph.

neural network has 16 hidden layer units with radial basis activation function, with the centers of the radial basis functions evenly distributed in $[-1, 1]$ and their variance is set as 1. The neural network control gains are chosen as $k_1 = 100$, $k_2 = 200$, $k_3 = 400$, $G = 10I_n$, $\kappa = 0.1$, $R = 20I_n$, $\rho = 0.01$. The neural network weights are initialized to zero. Determining the number of hidden layer units is an open problem. Computer simulations can be performed, with an increase in number of nodes for the next run. When no further improvement in controller performance is detected, that value of hidden layer nodes can be used. Increasing the number of neural network nodes will however increase the computation time of the code.

The communication digraph illustrated in Fig. 4 should be a graph containing a spanning tree such that each DG requires its own information and that of other neighbours. An optimization criteria to connect the DGs in an optimal way can be achieved by considering an objective such as minimizing the length of the communication link.

A static load model that expresses the power dependence with voltage as an exponential function has been utilized in the simulation, which is given by [28]:

$$P = P_o \left(\frac{V}{V_o}\right)^{np} \tag{38}$$

$$Q = Q_o \left(\frac{V}{V_o}\right)^{nq} \tag{39}$$

where P and Q are the load active and reactive power, respectively; P_o and Q_o are the active and reactive power consumed at rated voltage V_o respectively. By setting the exponents np and nq to 0, 1 or 2, the load model can represent a constant power, constant current or constant impedance load, respectively.

A. Case 1: Restoring Voltage and Frequency

The nominal voltage and frequency v_n and ω_n are set at 230 V (per phase RMS) and 314.16 rad/s (50 Hz), respectively. For case 1, all loads were modelled as constant impedance loads (i.e., np and nq are set to 2 for all loads). The multi-microgrid is assumed to be islanded at t = 0 s with only the conventional primary droop control active. The NN controller with droop maintains the frequency and voltage of the DGs at steady-state values after 0.3 s as seen in Fig. 5(a) and (b). The active power is also shared proportionally according to the ratings of the DGs. The primary droop control however exhibits voltage and frequency deviations from the nominal or set reference values. At $t = 0.5$ s, the secondary controller is activated. From Fig. 5(a), the neural network voltage control restores the voltage close to 1 pu while maintaining good reactive power sharing among the DGs. The neural network therefore approximates the DG dynamics well and does not affect the synchronization of the voltage magnitudes. The DG frequencies and output powers before and after applying the NN frequency controller is shown in Fig. 5(b) and (c). The DG frequencies are restored to 50 Hz after 0.3 s while sharing the active power proportionally according the ratings of the DGs.

B. Case 2: Effects of Load Types and Dynamics on Controller Performance

For this case, the effectiveness of the proposed controller under load changes is evaluated. To simplify the simulation results, we only show the response of DG4 when a constant impedance load, a constant current load and a constant power load of (15 kW, 6 kVAr) is added at its bus at $t = 0.5$ s. From Fig. 6, the additional loads cause voltage and frequency dips. Without knowledge of load dynamics, the adaptive neural network restores the voltage, frequency, active and reactive powers to steady-state values in about 0.3 s. The secondary controller is activated at $t = 1$ s to correct the voltage and frequency de-

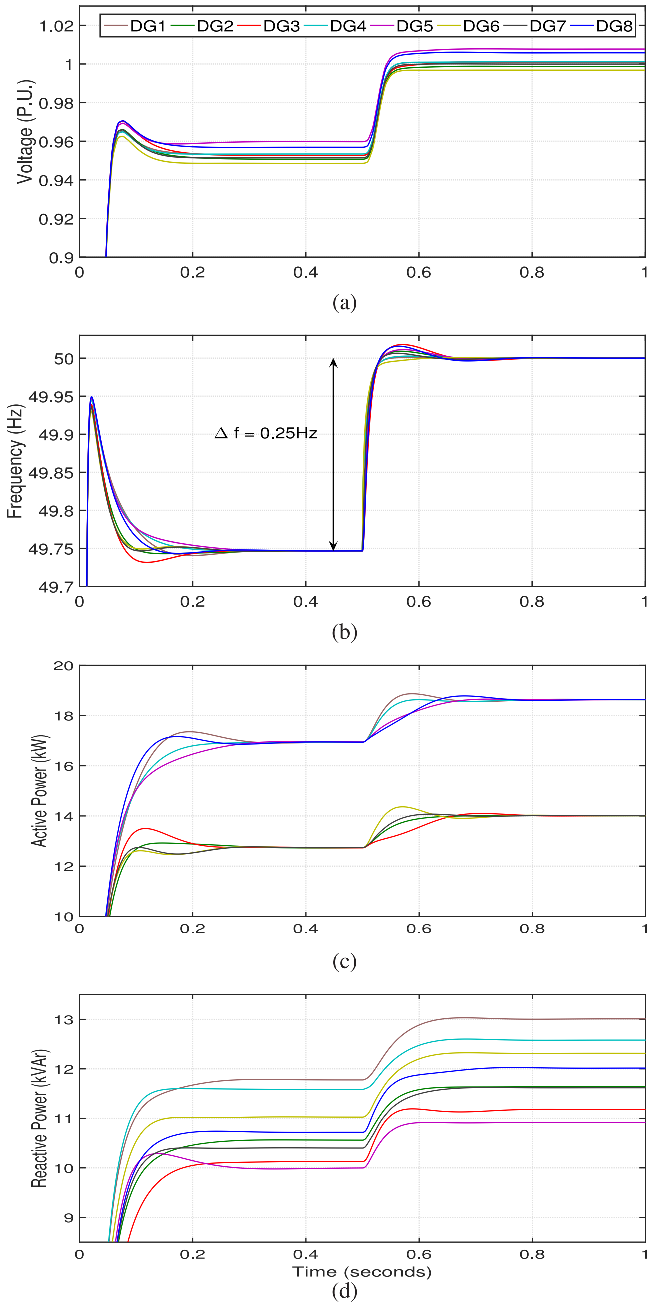

Fig. 5. DGs' responses for case 1. (a) DGs' output voltages. (b) DGs' frequencies. (c) DGs' active powers. (d) DGs' reactive powers.

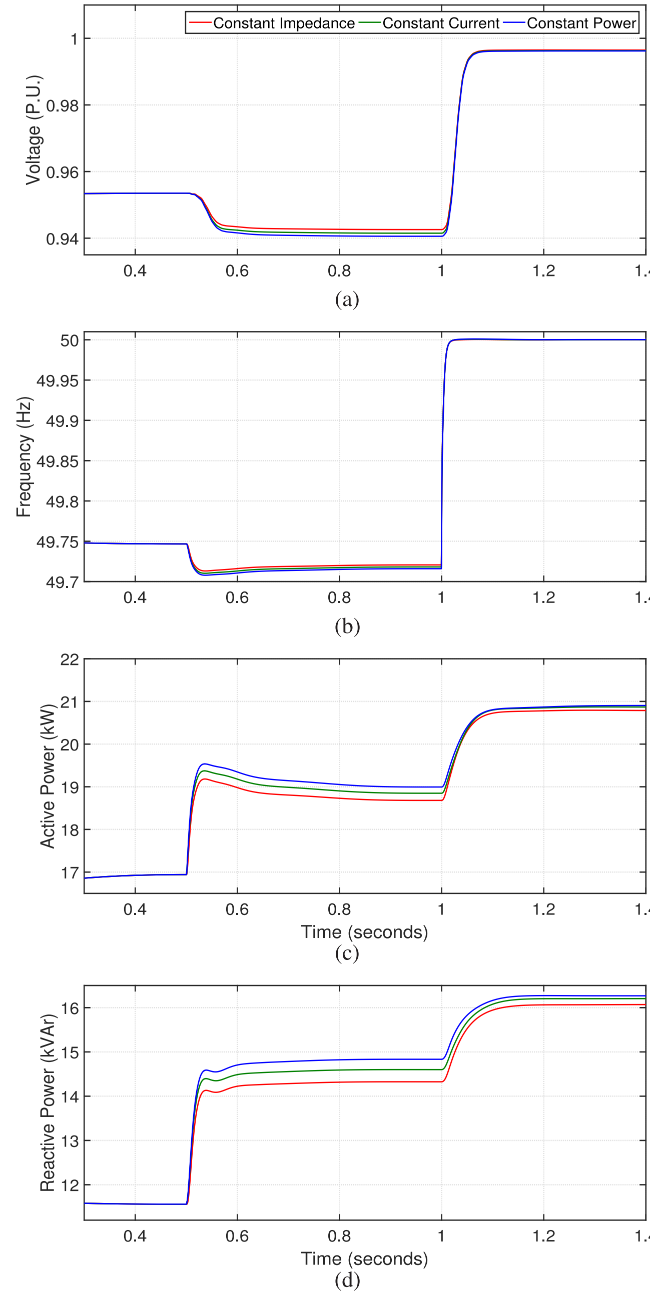

Fig. 6. Case 2 - DG 4 responses under different load types. (a) Output voltage. (b) Frequency. (c) Active power. (d) Reactive powers.

viations caused by the primary controller. The adaptive voltage and frequency controllers perform remarkably well by sharing the active and reactive powers of the loads among the DGs in about 0.3 s, while maintaining the voltage and frequency near nominal values. Fig. 7 shows the controller performance when a 15 kW induction motor is switched on at bus 4 and started with only 10% full load torque. The motor draws high amount of reactive power for a short period during its startup which causes voltage dips at the buses. The secondary controller is activated at $t = 1.2$ s, which restores the frequency and voltage to nominal values. The loading of the motor is increased to 40% and 90% at $t = 1.6$ s and $t = 2.15$ s, respectively. From Fig. 7, it is seen that the proposed controller shows good performance during induction motor load disturbances.

C. Case 3: Effects of Control Gains

From (45) and (52), choosing large values of k_{2i} and k_{3i} reduces $\|e_{2i}\|$ and $\|e_{\omega i}\|$, which in turn increases the synchronization speed and the response of the controllers. To show the effect of these gains on the speed response of the neural network controllers, the controller gains are set as $k_{1i} = 10$, $k_{2i} = 100$, $k_{3i} = 50$. The secondary control is activated at $t = 0.75$ s. From Fig. 8(a), it is seen that the voltage controller has a slower response speed with less overshoot than the case in Fig. 5(a),

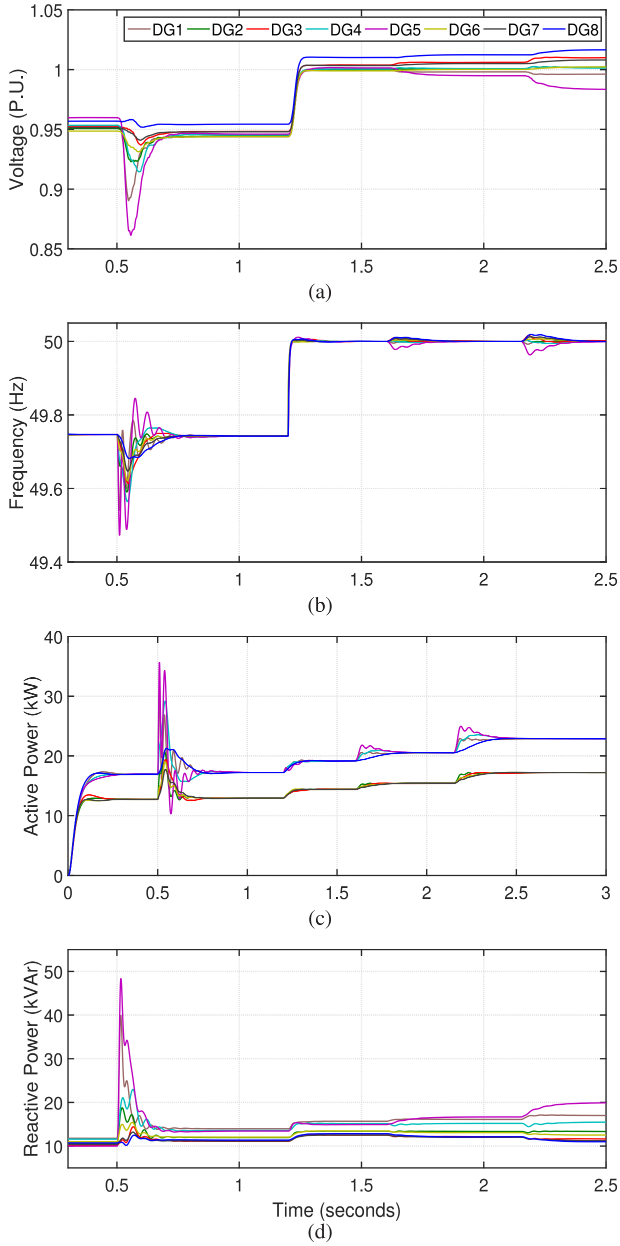

Fig. 7. Case 2 - DGs' responses when an induction motor load is switched on. (a) DGs' output voltages. (b) DGs' frequencies. (c) DGs' active powers. (d) DGs' reactive powers.

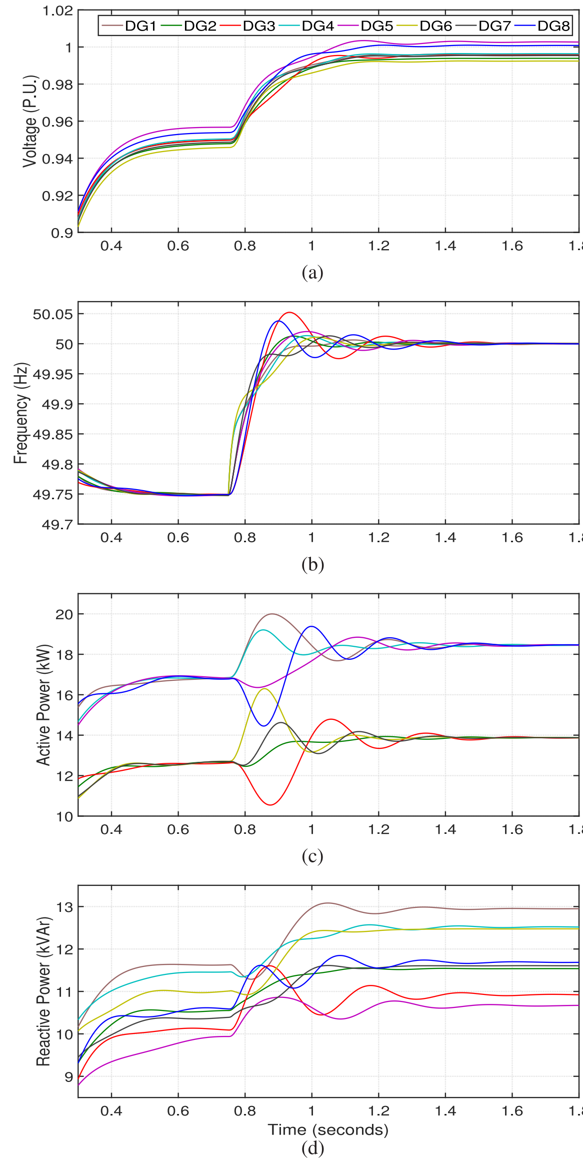

Fig. 8. DGs' responses for case 3. (a) DGs' output voltages. (b) DGs' frequencies. (c) DGs' active powers. (d) DGs' reactive powers.

where higher control gains were chosen. The frequency controller and output powers of the DGs in Fig. 8(b) and (c), also have a slower convergence rate compared to those in Fig. 5(b) and (c).

D. Case 4: Comparing the Proposed Controller Performance With Controller in [7]

To show the effectiveness of the proposed controller, a comparison is made with the primary and secondary voltage and frequency control schemes presented in [7]. The control method in [7], like most proposed microgrid control schemes in the literature, consists of an outer voltage controller and an inner current controller which uses conventional PI regulators to track DG voltages with respect to a reference value. The secondary controller presented in [7] is fully distributed such that each DG only requires its own information and the information of its neighbours using a communication digraph. In our paper, we utilize adaptive neural networks to develop an intelligent controller for both primary and secondary control actions of the microgrid. Therefore, the proposed controllers do not require the use of voltage and current PI controllers, which are usually difficult to tune at various operating conditions.

Due to the differences in secondary voltage control objectives between our proposed method and the method presented in [7], we only compare the performance of the PI regulator-based primary voltage control, primary frequency control and secondary frequency control in [7] with our proposed method. In order to account for the effect of load types and dynamics, different load types are considered in the simulated study case as

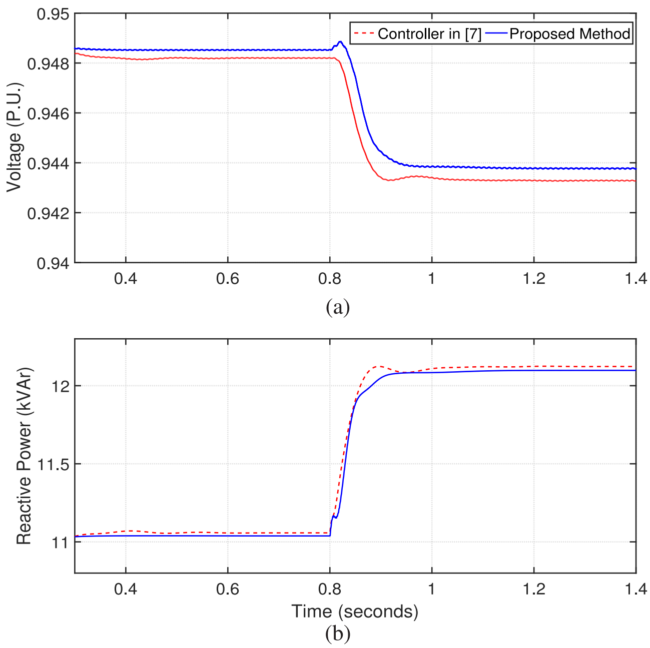

Fig. 9. Case 4 - Comparison of DG2 responses utilizing different primary controllers. (a) Voltage. (b) Reactive power.

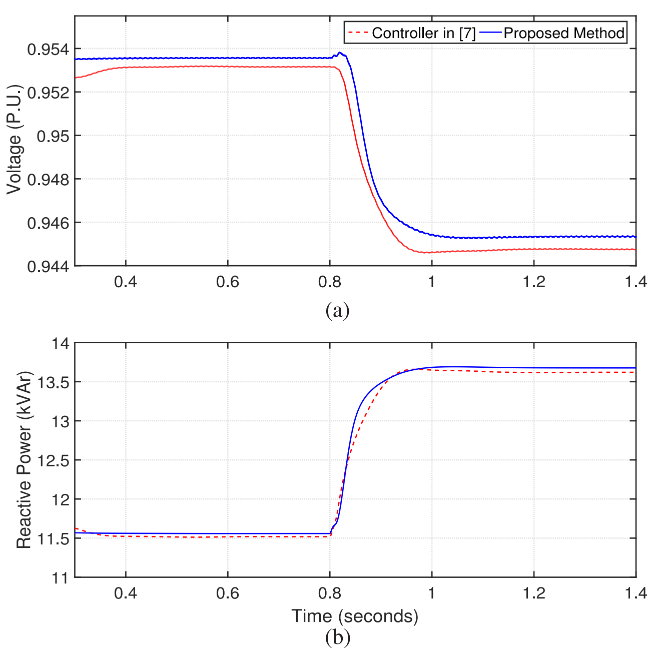

Fig. 10. Case 4 - Comparison of DG8 responses utilizing different primary controllers. (a) Voltage. (b) Reactive power.

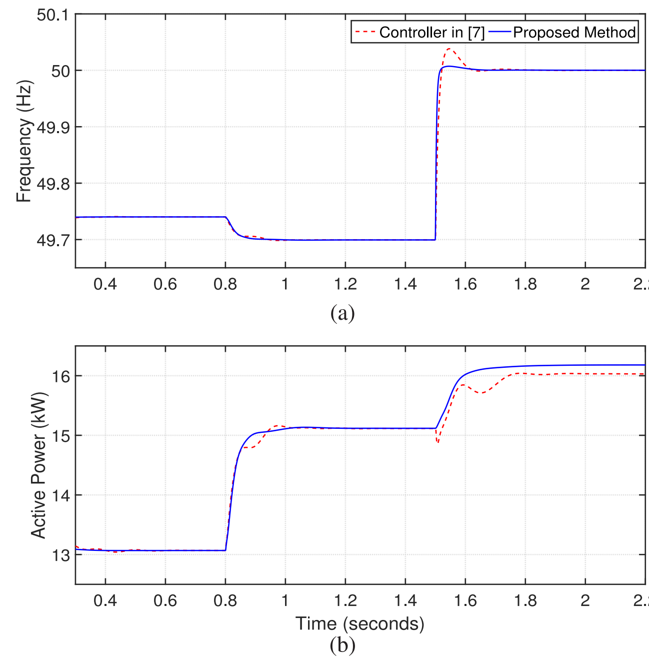

Fig. 11. Case 4 - Comparison of DG2 responses utilizing different primary and secondary controllers. (a) Frequency. (b) Active power.

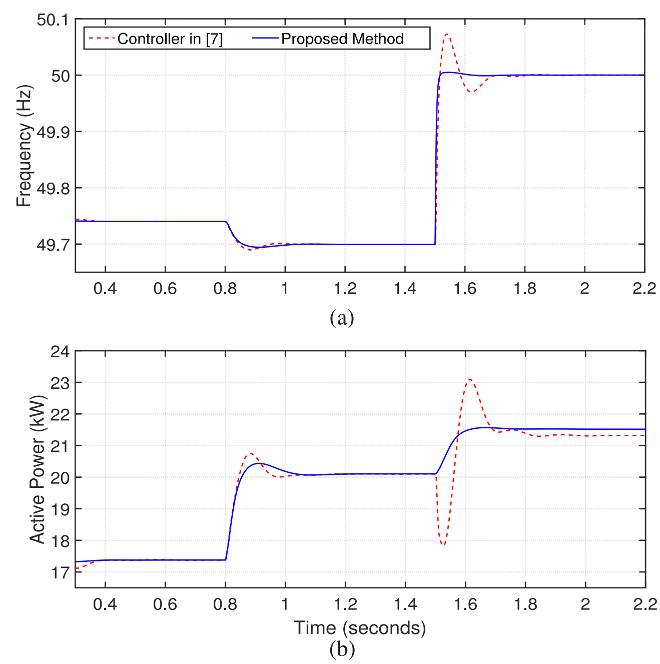

Fig. 12. Case 4 - Comparison of DG8 responses utilizing different primary and secondary controllers. (a) Frequency. (b) Active power.

well. For this comparison, loads 1 and 7 are constant impedance loads; loads 2, 4 and 6 are constant power loads, while loads 3, 5 and 8 are constant current loads. The ratings of these loads are given in Table II. At $t = 0.8$ s, while the primary controller is still active, additional loads of (5 kW, 5 kVAr, constant impedance), (10 kW, 6.5 kVAr, constant power) and (7 kW, 4.3 kVAr, constant current) were added to buses 1, 4 and 7, respectively. The addition of loads at different buses leads to voltage and frequency drops at all buses. To simplify the results, we only show the responses of DG 2 and DG 8. From Figs. 9–12, it can be seen that the DGs utilizing the proposed controller achieve superior frequency and active power regulations. The voltage, frequency, active power and reactive power also reach steady-state values in about 0.1 s faster than the PI control scheme. At $t = 1.5$ s, the secondary control is activated to correct the frequency deviations caused by the primary control as shown in Figs. 11 and 12. It can be observed that the proposed frequency controller shares the active power among the DGs, restores the frequency

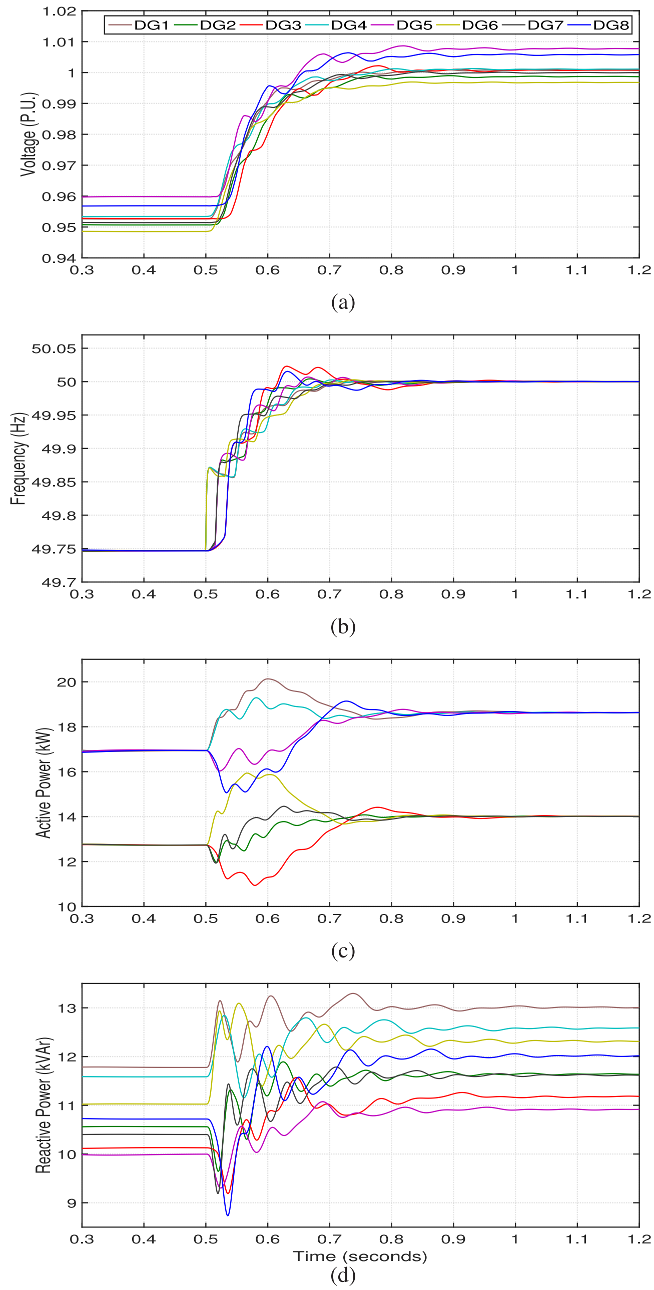

Fig. 13. DGs' responses for case 5. (a) DGs' output voltages. (b) DGs' frequencies. (c) DGs' active powers. (d) DGs' reactive powers.

to 50 Hz with less overshoot, and has a faster response speed than the control scheme presented in [7].

E. Case 5: Effects of Communication Delay

Communication plays an important role when a distributed controller is used. A fixed communication latency of 15 ms is considered for the distributed secondary voltage and frequency controllers. Control gains used in case 1 are used for this case as well. The secondary control action is applied at t = 0.5 s. From Fig. 13, it is seen that the controllers exhibit larger fluctuations. However, the output signals return to steady-state values in about 0.5 s.

V. Conclusion

In this paper, adaptive voltage and frequency controllers are developed for inverter-based DGs in a multi-microgrid structure using distributed cooperative control and neural networks. The proposed controllers are less dependent on system dynamics, maintain the voltage and frequency of the DGs near nominal values and share the active powers proportionally among the DGs. The effectiveness of the proposed controllers are verified under different scenarios, including sudden load changes, effect of different load types and dynamics, and the effects of control gains and communication delays. Further work includes development and implementation of controllers that compensate for the effects of communication delays to guarantee stable operation of the multi-microgrid. In future work, we would also look into how the proposed method will perform during faults and its effect on a utilized protection scheme as well as fault-ride-through operation.

Appendix A
Proof of Theorem 1

The Lyapunov function below is selected considering the effects of $\tilde{W}$ on system stability.

$$V_{3i} = V_{2i} + \frac{1}{2}\tilde{W}_i G_i^{-1}\tilde{W}_i \tag{40}$$

Differentiating (40) and substituting (26) and (27) yields

$$\begin{aligned}\dot{V}_{3i} &= \dot{V}_{2i} - \tilde{W}_i^T G_i^{-1}\dot{\hat{W}}_i \\ &= -k_{1i}e_{1i}^2 - k_{2i}e_{2i}^2 + \epsilon_i(x_i)e_{2i} + \kappa_i\|e_{2i}\|\tilde{W}_i^T\hat{W}_i \end{aligned}\tag{41}$$

$\tilde{W}_i^T\hat{W}_i$ can be expressed as

$$\begin{aligned}\tilde{W}_i^T(W_i - \tilde{W}_i) &= \tilde{W}_i^T W_i - \tilde{W}_i^T\tilde{W}_i \\ &\leq \|\tilde{W}_i\|_F\|W_i\|_F - \|\tilde{W}_i\|_F^2 \end{aligned}\tag{42}$$

V_{3i} therefore yields

$$\begin{aligned}\dot{V}_{3i} \leq & -k_{1i}\|e_{1i}\|^2 - \|e_{2i}\|\Big[k_{2i}\|e_{2i}\| - \epsilon_{n_v} \\ & + \kappa_i\|\tilde{W}_i\|_F(\|\tilde{W}_i\|_F - W_{\beta_v})\Big]\end{aligned}\tag{43}$$

$\dot{V}_{3i}$ is negative as long as the terms in the square brackets are positive. By completing the squares, the expression in the square brackets can be expressed as

$$k_{2i}\|e_{2i}\| - \epsilon_{n_v} - \kappa_i\frac{W_{\beta_v}^2}{4} + \kappa_i\left(\|\tilde{W}_i\|_F - \frac{W_{\beta_v}}{2}\right)^2. \tag{44}$$

From the above expression, V_{3i} is guaranteed to be negative as long as either

$$\|e_{2i}\| > \frac{\frac{\kappa_i W_{\beta_v}^2}{4} + \epsilon_{n_v}}{k_{2i}} \equiv \Omega_{e_{2i}} \quad \text{or} \tag{45}$$

$$\|\tilde{W}_i\|_F > \frac{W_{\beta_v}}{2} + \sqrt{\frac{W_{\beta_v}^2}{4} + \frac{\epsilon_{n_v}}{\kappa_i}} \equiv \Omega_{\tilde{W}_i}. \tag{46}$$

Thus, $\dot{V}_{3i}$ is negative outside a compact set. According to Lemma 1, $\|e_{2i}\|$ and $\|\tilde{W}_i\|_F$ are therefore bounded. Since e_{2i} is bounded, the local neighbourhood error e_{1i} is also bounded. Also, $\|e_{2i}\|$ can be made small by increasing the gain k_{2i}.

APPENDIX B
PROOF OF THEOREM 2

The function below is selected considering the effects of $\tilde{W}_{fi}$ on system stability.

$$V_4 = V_{fi} + \frac{1}{2}\tilde{W}_{fi} R_i^{-1} \tilde{W}_{fi}. \tag{47}$$

Differentiating (47) yields

$$\dot{V}_4 = \dot{V}_{fi} - \tilde{W}_{fi} R_i^{-1} \dot{\hat{W}}_{fi}. \tag{48}$$

Substituting (35) and (37) into (48) yields

$$\dot{V}_4 = -k_{3i} e_{\omega_i}^2 + \epsilon_i(x_{fi}) e_{\omega i} + \rho_i \|e_{\omega i}\| \tilde{W}_{fi}^T \hat{W}_{fi}. \tag{49}$$

Using the inequality $\tilde{W}_{fi}^T \hat{W}_{fi} \le \|\tilde{W}_{fi}\|_F \|W_{fi}\|_F - \|\tilde{W}_{fi}\|_F^2$, $\dot{V}_4$ is expressed as

$$\dot{V}_4 \le -\|e_{\omega i}\| \Bigg[k_{3i}\|e_{\omega i}\| - \epsilon_{n_f} + \rho_i \tilde{W}_{fi}\|_F (\|\tilde{W}_{fi}\|_F - W_{\beta_f}) \Bigg] \tag{50}$$

$\dot{V}_4$ is negative as long as the terms in the square brackets are positive. Completing the squares, these terms can be expressed as

$$k_{3i}\|e_{\omega i}\| - \epsilon_{n_f} - \rho_i \frac{W_{\beta_f}^2}{4} + \rho_i \left(\|\tilde{W}_{fi}\|_F - \frac{W_{\beta_f}}{2} \right)^2. \tag{51}$$

From the above expression, V_{4i} is guaranteed to be negative as long as either

$$\|e_{\omega i}\| > \frac{\frac{\rho_i W_{\beta_f}^2}{4} + \epsilon_{n_f}}{k_{3i}} \equiv \Omega_{e_{\omega i}} \tag{52}$$

or

$$\|\tilde{W}_{fi}\|_F > \frac{W_{\beta_f}}{2} + \sqrt{\frac{W_{\beta_f}^2}{4} + \frac{\epsilon_{n_f}}{\rho_i}} \equiv \Omega_{\tilde{W}_{fi}}. \tag{53}$$

Thus, $\dot{V}_{4i}$ is negative outside a compact set. According to Lemma 1, $\|e_{\omega i}\|$ and $\|\tilde{W}_{fi}\|_F$ are therefore bounded. Also, $\|e_{\omega i}\|$ can be made small and closer to zero by increasing the gain k_{3i} and hence ω_i synchronizes to ω_{ref}.

REFERENCES

[1] J. M. Guerrero, M. Chandorkar, T. L. Lee, and P. C. Loh, "Advanced control architectures for intelligent microgrids;part I: Decentralized and hierarchical control," *IEEE Trans. Ind. Electron.*, vol. 60, no. 4, pp. 1254–1262, Apr. 2013.

[2] X. Yang, Y. Du, J. Su, L. Chang, Y. Shi, and J. Lai, "An optimal secondary voltage control strategy for an islanded multibus microgrid," *IEEE J. Emerg. Sel. Topics Power Electron.*, vol. 4, no. 4, pp. 1236–1246, Dec. 2016.

[3] G. Chen and E. Feng, "Distributed secondary control and optimal power sharing in microgrids," *IEEE/CAA J. Autom. Sinica*, vol. 2, no. 3, pp. 304–312, Jul. 2015.

[4] L. Che, M. Shahidehpour, A. Alabdulwahab, and Y. Al-Turki, "Hierarchical coordination of a community microgrid with ac and dc microgrids," *IEEE Trans. Smart Grid*, vol. 6, no. 6, pp. 3042–3051, Nov. 2015.

[5] D. E. Olivares *et al.*, "Trends in microgrid control," *IEEE Trans. Smart Grid*, vol. 5, no. 4, pp. 1905–1919, Jul. 2014.

[6] A. Bidram, A. Davoudi, and F. L. Lewis, "A multiobjective distributed control framework for islanded ac microgrids," *IEEE Trans. Ind. Informat.*, vol. 10, no. 3, pp. 1785–1798, Aug. 2014.

[7] A. Bidram, A. Davoudi, F. L. Lewis, and Z. Qu, "Secondary control of microgrids based on distributed cooperative control of multi-agent systems," *IET Transm. Gener. Distrib.*, vol. 7, no. 8, pp. 822–831, Aug. 2013.

[8] J. W. Simpson-Porco, Q. Shafiee, F. Drfler, J. C. Vasquez, J. M. Guerrero, and F. Bullo, "Secondary frequency and voltage control of islanded microgrids via distributed averaging," *IEEE Trans. Ind. Electron.*, vol. 62, no. 11, pp. 7025–7038, Nov. 2015.

[9] Y. Han, H. Li, P. Shen, E. A. A. Coelho, and J. M. Guerrero, "Review of active and reactive power sharing strategies in hierarchical controlled microgrids," *IEEE Trans. Power Electron.*, vol. 32, no. 3, pp. 2427–2451, Mar. 2017.

[10] A. Bidram, A. Davoudi, F. L. Lewis, and J. M. Guerrero, "Distributed cooperative secondary control of microgrids using feedback linearization," *IEEE Trans. Power Syst.*, vol. 28, no. 3, pp. 3462–3470, Aug. 2013.

[11] A. Micallef, M. Apap, C. Spiteri-Staines, and J. M. Guerrero, "Secondary control for reactive power sharing in droop-controlled islanded microgrids," in *Proc. 2012 IEEE Int. Symp. Ind. Electron.*, May 2012, pp. 1627–1633.

[12] H. Mahmood, D. Michaelson, and J. Jiang, "Accurate reactive power sharing in an islanded microgrid using adaptive virtual impedances," *IEEE Trans. Power Electron.*, vol. 30, no. 3, pp. 1605–1617, Mar. 2015.

[13] A. Bidram, A. Davoudi, and F. L. Lewis, "Two-layer distributed cooperative control of multi-inverter microgrids," in *Proc. 2014 IEEE Appl. Power Electron. Conf. Expo*, Mar. 2014, pp. 2364–2371.

[14] W. He, A. O. David, Z. Yin, and C. Sun, "Neural network control of a robotic manipulator with input deadzone and output constraint," *IEEE Trans. Syst., Man, Cybern., Syst.*, vol. 46, no. 6, pp. 759–770, Jun. 2016.

[15] W. He, D. O. Amoateng, C. Yang, and D. Gong, "Adaptive neural network control of a robotic manipulator with unknown backlash-like hysteresis," *IET Control Theory Appl.*, vol. 11, no. 4, pp. 567–575, Feb. 2017.

[16] H.-C. Fu, H.-Y. Chang, Y. Y. Xu, and H. T. Pao, "User adaptive handwriting recognition by self-growing probabilistic decision-based neural networks," *IEEE Trans. Neural Netw.*, vol. 11, no. 6, pp. 1373–1384, Nov. 2000.

[17] S. Li, P. Wang, and L. Goel, "A novel wavelet-based ensemble method for short-term load forecasting with hybrid neural networks and feature selection," *IEEE Trans. Power Syst.*, vol. 31, no. 3, pp. 1788–1798, May 2016.

[18] N. Ding, C. Benoit, G. Foggia, Y. Bsanger, and F. Wurtz, "Neural network-based model design for short-term load forecast in distribution systems," *IEEE Trans. Power Syst.*, vol. 31, no. 1, pp. 72–81, Jan. 2016.

[19] A. Chatterjee and A. Keyhani, "Neural network estimation of microgrid maximum solar power," *IEEE Trans. Smart Grid*, vol. 3, no. 4, pp. 1860–1866, Dec. 2012.

[20] Y. A. R. I. Mohamed and E. F. El-Saadany, "Adaptive decentralized droop controller to preserve power sharing stability of paralleled inverters in distributed generation microgrids," *IEEE Trans. Power Electron.*, vol. 23, no. 6, pp. 2806–2816, Nov. 2008.

[21] N. Pogaku, M. Prodanovic, and T. C. Green, "Modeling, analysis and testing of autonomous operation of an inverter-based microgrid," *IEEE Trans. Power Electron.*, vol. 22, no. 2, pp. 613–625, Mar. 2007.

[22] V. Nasirian, S. Moayedi, A. Davoudi, and F. L. Lewis, "Distributed cooperative control of dc microgrids," *IEEE Trans. Power Electron.*, vol. 30, no. 4, pp. 2288–2303, Apr. 2015.

[23] Y. H. Kim and F. L. Lewis, "Output feedback control of rigid robots using dynamic neural networks," in *Proc. IEEE Int. Conf. Robot. Autom.*, Apr. 1996, vol. 2, pp. 1923–1928.

[24] F. Lewis, S. Jagannathan, and A. Yesildirak, *Neural Network Control of Robot Manipulators and Non-Linear Systems*. Boca Raton, FL, USA: CRC Press, 1998.

[25] X. Wu, C. Shen, and R. Iravani, "A distributed, cooperative frequency and voltage control for microgrids," *IEEE Trans. Smart Grid*, to be published.

[26] F. Lewis, A. Yesildirek, and K. Liu, "Multilayer neural-net robot controller with guaranteed tracking performance," *IEEE Trans. Neural Netw.*, vol. 7, no. 2, pp. 388–399, Mar. 1996.

[27] I. P. Nikolakakos, H. H. Zeineldin, M. S. El-Moursi, and N. D. Hatziargyriou, "Stability evaluation of interconnected multi-inverter microgrids through critical clusters," *IEEE Trans. Power Syst.*, vol. 31, no. 4, pp. 3060–3072, Jul. 2016.

[28] K. Hatipoglu, I. Fidan, and G. Radman, "Investigating effect of voltage changes on static zip load model in a microgrid environment," in *Proc. North Amer. Power Symp.*, Sep. 2012, pp. 1–5.

David Ofosu Amoateng (S'15) received the B.Sc. degree in electrical/electronic engineering from the Kwame Nkrumah University of Science and Technology, Kumasi, Ghana, in 2013 and the M.Sc. degree in electronic science and technology from the University of Electronic Science and Technology of China, Chengdu, China, in 2016. He is currently working toward the Ph.D. degree in biorobotics at the Biorobotics Institute, Scuola Superiore Sant'Anna, Pisa, Italy. His research interests include robotics, intelligent control, signal processing, and machine learning.

Mohamed Al Hosani (S'10–M'13) received the B.Sc. degree in electrical engineering from the American University of Sharjah, Sharjah, United Arab Emirates, in 2008, and the M.Sc. and the Ph.D. degrees in electrical engineering from the University of Central Florida, Orlando, FL, USA, in 2010 and 2013, respectively. Since 2014, he has been with the Department of Electrical Engineering and Computer Science, Masdar Institute, Khalifa University of Science and Technology, Abu Dhabi, United Arab Emirates, as an Assistant Professor. He was a Visiting Assistant Professor at the Massachusetts Institute of Technology, Cambridge, MA, USA, for 8 months during 2015–2016. His current interests include antiislanding algorithm, distributed generation protection and control, and modeling and stability analysis of the microgrid.

Mohamed Shawky El Moursi (M'12–SM'15) received the B.Sc. and M.Sc. degrees from Mansoura University, Mansoura, Egypt, in 1997 and 2002, respectively, and the Ph.D. degree from the University of New Brunswick (UNB), Fredericton, Canada, in 2005, all in electrical engineering. He was a Research and Teaching Assistant with the Department of Electrical and Computer Engineering, UNB, from 2002 to 2005. He joined McGill University as a Postdoctoral Fellow with the Power Electronics Group. He joined Vestas Wind Systems, Arhus, Denmark, in the Technology R&D with the Wind Power Plant Group. He was with TRANSCO, UAE, as a Senior Study and Planning Engineer and second-ed to Associate Professor Position in the Faculty of Engineering, Mansoura University, Mansoura, Egypt and currently on leave. He is currently an Associate Professor in the Electrical Engineering and Computer Science Department, Masdar Institute, Khalifa University of Science and Technology. He was a Visiting Professor at Massachusetts Institute of Technology, Cambridge, MA, USA. His research interests include power system, power electronics, FACTS technologies, VSC-HVDC systems, microgrid operation and control, and renewable energy systems (wind and PV) integration and interconnections.

Dr. Shawky is currently an Editor of the IEEE TRANSACTIONS ON POWER DELIVERY, an Editor of the IEEE TRANSACTIONS ON POWER SYSTEMS, an Associate Editor of the IEEE TRANSACTIONS ON POWER ELECTRONICS, a Guest Editor of the IEEE TRANSACTIONS ON ENERGY CONVERSION, an Editor for IEEE POWER ENGINEERING LETTERS, a Regional Editor for *IET Renewable Power Generation*, and an Associate Editor for *IET Power Electronics Journals*.

Konstantin Turitsyn (M'09) received the M.Sc. degree in physics from the Moscow Institute of Physics and Technology, Dolgoprudny, Russia, and the Ph.D. degree in physics from the Landau Institute for Theoretical Physics, Moscow, Russia, in 2007. Currently, he is an Assistant Professor at the Mechanical Engineering Department of Massachusetts Institute of Technology (MIT), Cambridge, MA, USA. Before joining MIT, he held the position of Oppenheimer Fellow at Los Alamos National Laboratory, and KadanoffRice Postdoctoral Scholar at the University of Chicago. His research interests encompass a broad range of problems involving nonlinear and stochastic dynamics of complex systems. His main interests include energy-related fields include stability and security assessment, integration of distributed, and renewable generation.

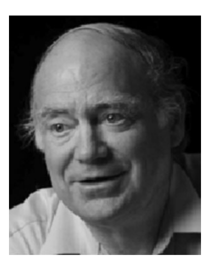

James L. Kirtley, Jr. (M'71–SM'80–F'91–LF'11) received the Ph.D. degree from the Massachusetts Institute of Technology (MIT), Cambridge, MA, USA, in 1971. Currently, he is a Professor of electrical engineering at MIT. He was with General Electric, Large Steam Turbine Generator Department, as an Electrical Engineer, for Satcon Technology Corporation as Vice President and General Manager of the Tech Center and as a Chief Scientist and as the Director. He was Gastdozent at the Swiss Federal Institute of Tech-nology, Zurich (ETH), Switzerland. He is a specialist in electric machinery and electric power systems.

Prof. Kirtley, Jr. served as Editor-in-Chief of the IEEE TRANSACTIONS ON ENERGY CONVERSION from 1998 to 2006 and continues to serve as an Editor for that journal and as a member of the Editorial Board of the journal *Electric Power Components and Systems*. He was awarded the IEEE Third Millennium medal in 2000 and the Nikola Tesla prize in 2002. He was elected to the United States National Academy of Engineering in 2007. He is a Registered Professional Engineer in Massachusetts, USA.